Three-Dimensional Laminar Boundary-Layer Transition on a Sharp 8° Cone at Mach 10

V. DiCristina*

Avco Corporation, Wilmington, Mass.

Wind-tunnel tests were conducted at the Arnold Engineering Development Center in the VKF Tunnel C facility at Mach 10 to obtain the spatial distribution of the boundary-layer transition zone on a sharp 8° half-angle cone. The boundary-layer transition line was obtained for small angles of attack at freestream Reynolds numbers of 1.5×10^6/ft and 2.1×10^6/ft. Mass addition effects on the transition movement also were obtained using a low-temperature subliming material to simulate the scaled mass injection rate of actual ablation materials. Body dynamic motion effects on transition stability were investigated at the amplitude and frequency levels observed in flight. The results of this study show that angle of attack and boundary-layer mass addition have first-order effects on transition behavior. Low-frequency body dynamic motion appears to have a second-order effect with respect to the cross flow transition distribution and a negligible effect on the axial transition location. Of significant importance is the observation of a transition reversal phenomenon with respect to the cross flow body distribution.

Nomenclature

C_p = specific heat
$\dot{m}$ = ablation rate
M = Mach number
$\dot{q}$ = heat flux
Re = Reynolds number
St = Stanton number
t = time
T = temperature
V = total velocity at the edge of the boundary layer along the cone surface
X = distance on the surface of the cone
α = angle of attack
θ = momentum thickness
ρ = density
τ = calorimeter thickness
ϕ = angular coordinate measured circumferentially around the cone
μ = Viscosity

Subscripts

e = conditions at the edge of the boundary layer
∞ = freestream conditions
0 = conditions at zero angle of attack
TR = transition location
W = wall
R = recovery
S = stagnation

I. Introduction

EXISTING flight test data and current ground test studies[1,2] have indicated that boundary-layer transition location has a significant effect on the aerodynamic behavior of slender conical re-entry bodies. Static and dynamic stability prediction analyses depend on the boundary-layer

state, whether laminar or turbulent, as well as the axial location and spacial distribution of the transition front. This transition behavior is further complicated by angle-of-attack effects, roughness, boundary-layer mass addition, and body dynamic motion.

The current literature includes experimental data on the unidirectional transition behavior with angle of attack.[3,4] Little ground test experimental data exists on boundary-layer transition with ablating walls, and three-dimensional transition data, except at low Mach numbers,[5] are practically nonexistent.

This paper presents the results of an extensive experimental program aimed at defining the spacial distribution and movement of the boundary-layer transition zone on a sharp conical body including the effects of angle of attack, mass addition, and body dynamic motion.

II. Experimental Equipment and Models

Facility

The wind-tunnel test program was conducted at the Tunnel C Facility of the Arnold Engineering Development Center. The flow environment for both the ablating and nonablating configurations was a freestream Mach 10 and freestream Reynolds numbers of 1.5×10^6/ft and 2.1×10^6/ft at a total temperature of 1900°R.

The aerothermodynamic test conditions of this facility are suitable for testing low-temperature sublimers such as paradichlorobenzene ($C_6H_4Cl_2$) as a means of simulating an ablating surface. The scaled mass injection rates for these tests were $\dot{m}/\rho_\infty$ V_∞ A = 0.009 at $R_{e\infty}$ = 1.5 $\times$ 10^6 ft^{-1}
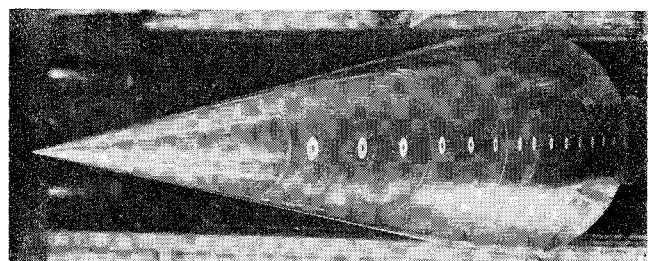

Fig. 1 Model installation in tunnel C of VKF facility.

and $\dot{m}/\rho_\infty \, V_\infty \, A = 0.012$ at $R_{e\infty} = 2.1 \times 10^6 \, \text{ft}^{-1}$. For the flight case at altitudes of interest $\dot{m}/\rho_\infty \, V_\infty \, A$ varies between 0.01–0.05.

Model Description

The external test configuration was a sharp, eight degree half-angle cone having a 10-in. base diam. The two configurations tested, one ablative and the other nonablative, had identical external geometries.

The nonablating heat-transfer model, as shown in Fig. 1, had an electroformed nickel skin 0.060-in. thick. A solid steel nose was provided to bring the model contour to a sharp tip. The model was instrumented with 30 capacitance-type heat-transfer gages on two rays 180° apart. Each ray contained 15 heat gages equally spaced about two inches apart.

The heat gages consist of 0.050-in. thick stainless steel discs which were pressed into an insulating DELRIN sleeve. Chromel-alumel thermocouples were spot welded to the inside surface of the thin metal disc and 30-ft leads secured to the stem of the heat gage with potting compound as shown in Fig. 2.

The ablative model as shown in Fig. 3 was identical in external geometry to the nonablative model and was fitted with interchangeable ablative shells. The ablative shells were fabricated of two conical frustrums which were held onto the model by a solid nose piece. The materials used in the ablative shell construction were paradichlorobenzene ($C_6H_4Cl_2$) plus four percent polyethylene. A change of ablative shell was required for each data run.

III.   Test Technique

The transition location was observed using a shadowgraph system with two microsecond spark duration providing an instantaneous picture of the state of the boundary layer. The shadowgraph system was fixed to record the upper and lower meridian lines of the model; a suitable means of rotation was necessary so that the meridian lines containing the calorimeter gages always remained in the vertical plane for all angles of attack, while the model displayed various peripheral locations. To obtain this orientation, a wedge of the same angle as the angle of attack was inserted between the model and the tunnel support systems. Then the model support system, along with the wedge, was rotated to the desired peripheral angles and the model was counter-rotated about its axis by the same angle to orient the calorimeter gages into the viewing plane. This technique enabled both the heat-transfer and optical measurement of the boundary-layer state to be made simultaneously. The boundary-
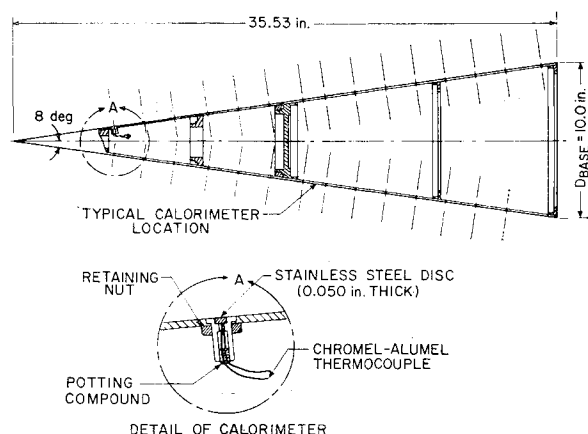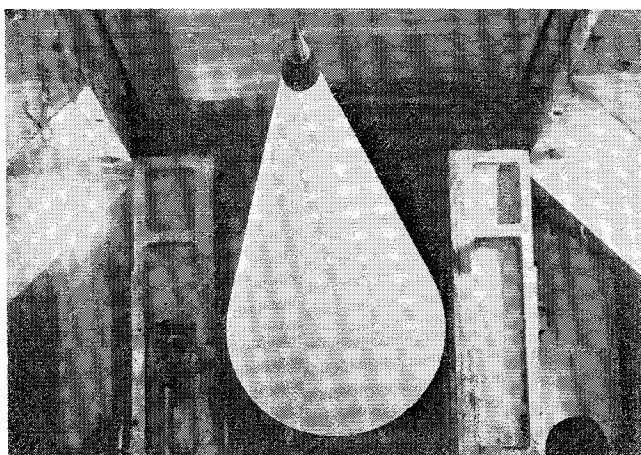

Fig. 3   Typical ablative model installation.

layer transition line was observed for the 0°, 36°, 72°, and 90° meridians and their corresponding opposite angles (180°, 216°, 252°, and 270°).

To simulate the ablating surface, the test model was provided with a paradichlorobenzene shell 0.20 in. thick. The average rate of mass addition to the boundary layer was determined from pretest and post-test weights of ablating shells and the time the model remained in the flow. The ablating model was not equipped with heat-transfer instrumentation. The low phase change temperature of para-dichlorobenzene (587°R) enables steady-state ablation to be achieved very rapidly. From heat-transfer calculations and earlier tests performed in this facility it takes about 0.15 sec. to obtain steady-state ablation conditions at zero angle of attack. For the 4° angle-of-attack case the windward side stabilizes in about 0.10 sec while the leeward side takes 0.30 sec. The shadowgraph pictures were taken 0.5–3.0 sec after the model was centered in the flow stream representing a period of steady-state ablation. Model dimensional changes during the data taking period were negligible. The highest turbulent heating condition resulted in a calculated dimensional mass loss of 0.004 in. after 3 sec of exposure, an amount which could not be measured in the photographs and which represented a negligible change in model configuration.

The dynamic phase of the tests was conducted using the same models mounted on a forced oscillation mechanism which had the capability of maintaining a constant amplitude of oscillation. The oscillating frequency was held constant at two cycles per second. The models were forced to oscillate at constant amplitudes of 1, 2, and 3 degrees maintaining the same positions to the flow as in the previous phase. The boundary-layer transition was observed using the same shadowgraph system as before with the observations recorded at peak amplitude.

At least four transition locations (X_{TR}) were obtained for each model attitude and position. A shadowgraph was obtained as soon as the model was injected in the flow and about three seconds later another shadowgraph was taken; then the model was retracted from the flow and cooled. This procedure was then repeated a second time. The results were numerically averaged giving a value of X_{TR} for a particular model attitude and flow condition. Thus a composite picture of the average boundary-layer transition line was
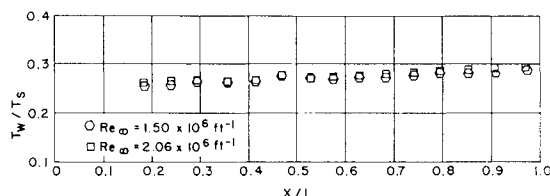

Fig. 2   Model configuration and calorimeter detail.

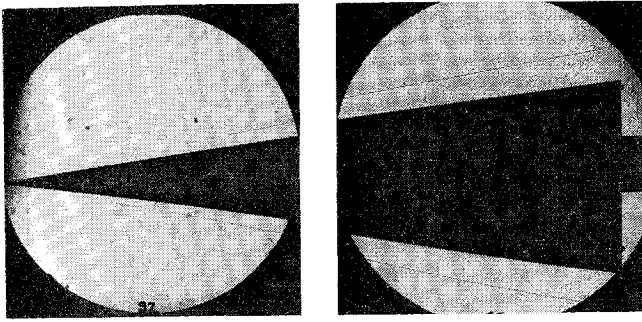**Fig. 4   Model wall temperature distribution.**

Fig. 5   Typical shadowgraph of nonablating model.

obtained for each test condition. The average wall temperature ratio was 0.27 which was nearly constant over the body length as shown in Fig. 4.

The temperature time history of each calorimeter was recorded on magnetic tape every 0.05 sec for about 5 sec. The time interval over which data was taken was divided into three segments and a least square curve fit was applied to the data points in these segments. The rate of tempera-
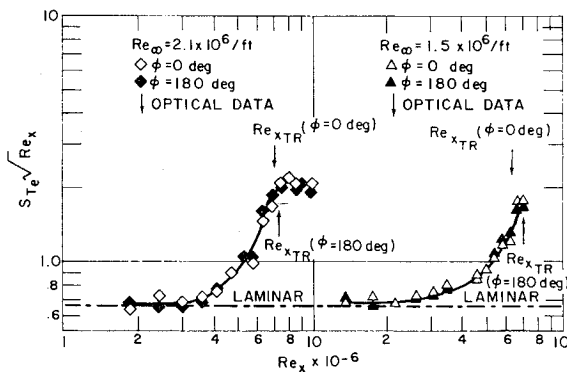

Fig. 6   Heat-transfer rate at $\alpha = 0°$ and $\phi = 0°$.

ture change (dT/dt) was calculated for the linear portion of the temperature response curve. The heat flux was then calculated from the expression $\dot{q} = \rho C_p \tau (dT/dt)$.

IV.   Results

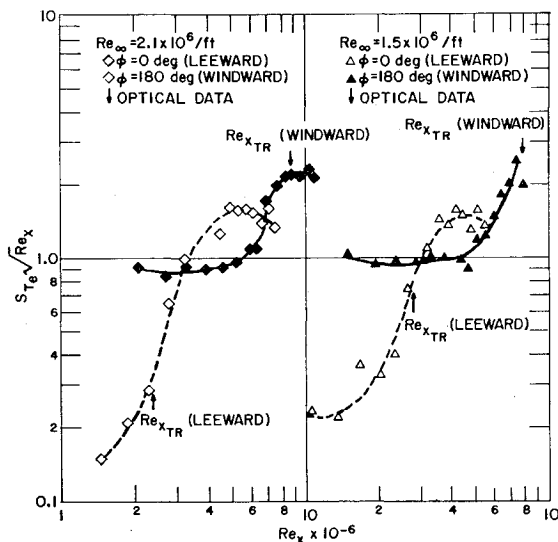The measurement of optical transition data is generally open to interpretation. Figure 5 represents a typical shadow-

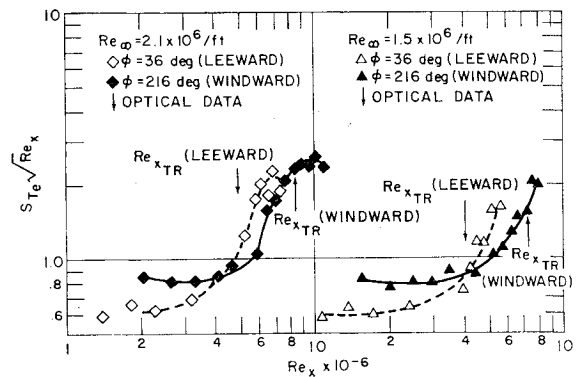Fig. 7   Heat-transfer rate at $\alpha = 4°$ and $\phi = 0°$.

Fig. 8   Heat-transfer rate at $\alpha = 4°$ and $\phi = 36°$.

graph revealing the detailed structure of the boundary layer over the top and bottom generators. The original photographs show the laminar region as a thin white line with increasing distance from the cone surface as it sweeps aft. As the line proceeds toward the turbulent region, the sharpness diminishes and then totally disappears in what seems to be the fully developed turbulent region. The end of transition is defined optically where this line disappears. The beginning and end of transition is defined more explicitly through heat-transfer measurements. Figure 6 shows a typical heat-transfer distribution along the body length indicated as the local Reynolds number Re_x. The laminar heat-transfer coefficient $St_e(Re_x)^{1/2}$ agrees well with predicted compressible value. The beginning of transition is clearly indicated as the increase in heat-transfer over the laminar value. The end of transition or the point where fully developed turbulent flow is established is the peak in the heat-transfer curve. The optically observed transition point as described previously nearly coincides with the point of fully developed turbulent flow or the end of transition. In almost all the cases the optical results indicated transition at a lower Reynolds number than the peak of the heat-transfer data. Detailed observations of the boundary-layer state in the vicinity where the heat transfer measurement begins to increase above the laminar condition indicates a region of faint turbulent "bursts." These short turbulent bursts increase in strength as they are swept aft, terminating in the turbulent boundary layer. Figures 7–10 show the variation of heat-transfer around and along the conical body for the 4° angle-of-attack case. With increasing angle of attack the transition movement undergoes a much more rapid forward progression on the leeward side than the rearward progression for the windward side. Figure 11 indicates the shift of the optically observed transition locations. For the angle-of-attack case, the observation that the optical transition point was the end of transition appears to hold for the windward generator, but is not representative
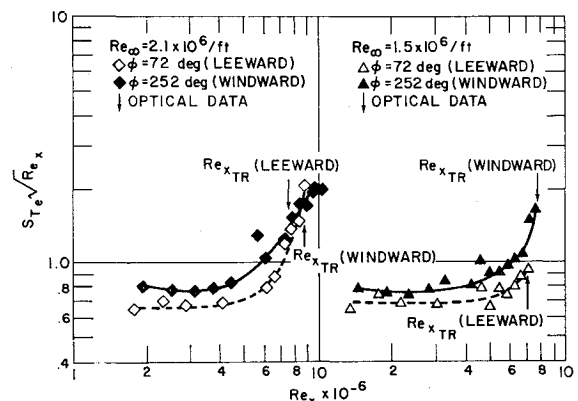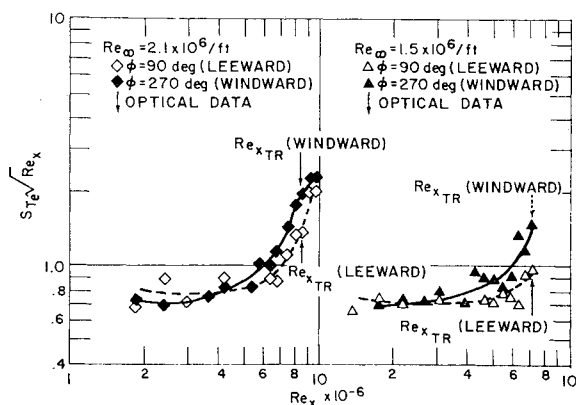

Fig. 9   Heat-transfer rate at $\alpha = 4°$ and $\phi = 72°$.

Fig. 10   Heat-transfer rate at $\alpha = 4°$ and $\phi = 90°$.

of the leeward generator as indicated in Fig. 7. Since no heat-transfer measurements were made for the ablating test cases, all the transition location comparisons presented are based on the optical measurements. In order to determine the meaningfulness of the optically derived transition distributions, the beginning of transition as determined from the heat-transfer data is shown in Fig. 12 and compared with the optical measurements. The general character of the transition distribution from beginning to end is generally preserved. The length of transitional flow varies
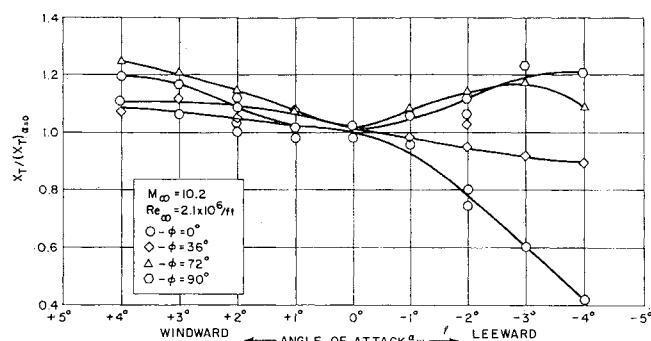

Fig. 11   Transition location at angle of attack.

around the body and is approximately equal to the length of laminar flow on the windward side and increases to about 1.6 times the laminar length at the 90° cross flow meridian. The spacial distribution of the boundary-layer transition point, for various angles of attack, is shown in Fig. 13 at two freestream Reynolds number conditions.

Since the local Mach number varies along the cone surface with angle of attack the change, in transition Reynolds number can be correlated with local Mach number as shown in Fig. 14. On the windward side the transition Reynolds number exhibits a linear behavior with Mach number,
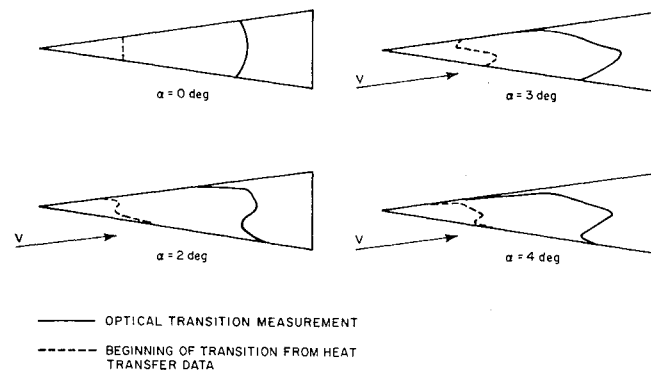

OPTICAL TRANSITION MEASUREMENT

BEGINNING OF TRANSITION FROM HEAT TRANSFER DATA

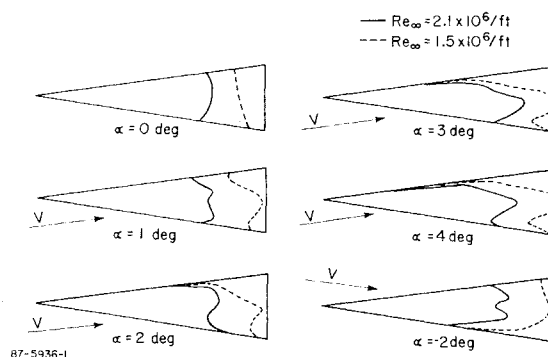Fig. 12   Comparison of optical and gage measured boundary-layer transition.

Fig. 13   Spacial distribution of boundary-layer transition.

however, on the leeward side it appears nonlinear as expected due to upwash effects. This transition Reynolds number—Mach number dependency—is consistent with other published data.[6] A comparison of the present data with other published sharp cone results at Mach 10 is shown in Fig. 15, after Ref. 7. The present data shown in Fig. 15 is the beginning of transition from the heat-transfer measurements at zero angle of attack. The transition Reynolds number based on $\bar{Re}_x$ cannot be correlated with local Mach number as was done in Fig. 14 since at angle of attack the strong cross flow velocity component is not accounted for.

Fig. 14   Transition Reynolds number as a function of local Mach number.
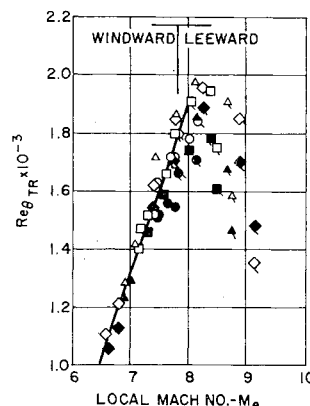
Boundary-layer mass addition has a significant effect on the transition location. It was generally observed that mass addition causes transition to occur at a lower Reynolds number but does not significantly alter the transition profile as shown in Fig. 16. The average forward movement of
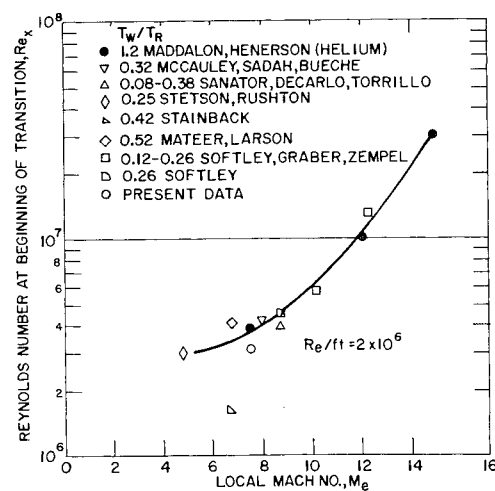

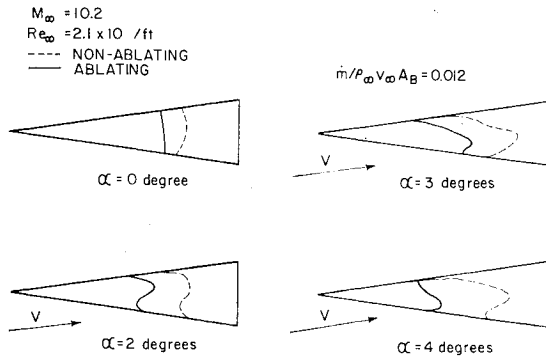Fig. 15   Transition Reynolds number correlation with other test data.

Fig. 16 Spacial distribution of boundary-layer transition with ablating and nonablating walls.

Fig. 19 Spacial distribution of boundary-layer transition for static and oscillating models with ablating wall.

the transition front due to mass transfer effects is shown to be nearly linear with angle of attack as indicated in Fig. 17. The data spread shown in Fig. 17 represents the peripheral variation of the transition points.

Planar oscillatory motion, up to the amplitude and frequency levels tested, appears to have only minor effects on transition location. Figures 18 and 19 show the oscillating model transition profiles for both the nonablating and ablat-
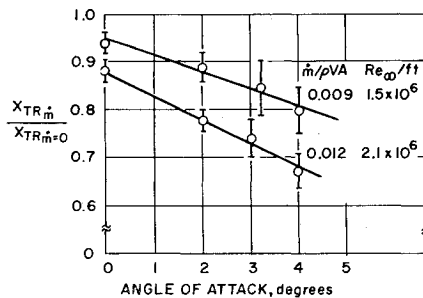

Fig. 17 Angle-of-attack and mass addition effects on transition location.

ing wall conditions as compared to the corresponding static body results.

V. Conclusions

This study has shown that angle-of-attack and boundary-layer mass transfer rate have a significant effect on the transition behavior. Mass addition has a more destabilizing influence than body dynamic motion. Low-frequency body
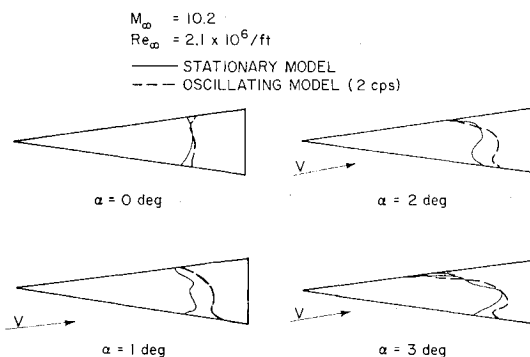

Fig. 18 Spacial distribution of boundary-layer transition for static and oscillating models with nonablating wall.
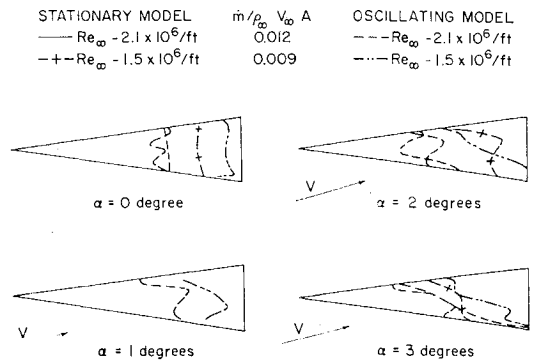
motion had a minor effect on the cross flow transition distribution and a negligible effect on the axial transition location. In almost all cases, at angles of attack, the peripheral transition profile was grossly nonlinear exhibiting a persistent reversal pattern.

It is of interest also to note some of the pertinent observations which could be important in the interpretation of present and future transition data: 1) optical transition measurements compare more nearly to the point where fully developed turbulent flow exists; 2) at angle of attack, the leeward side optical transition measurements neither indicates the beginning or the end of transition; 3) optical sighting of turbulent bursts coincides with the initial increase in the measured heat-transfer rate and the transition onset point; 4) with angle of attack the leeward transition point moves forward much more rapidly compared to the nearly static windward generator; and 5) the transition zone, from the onset of transition to fully turbulent flow, extends nearly one half the body length and represents a transition Reynolds number about half that for fully turbulent flow. Similar results were observed from flight test data and are described in Ref. 8.

References

[1] Ward, L. K., "Influence of Boundary Layer Transition on Dynamic Stability at Hypersonic Speeds," *Transaction of the Second Technical Workshop on Dynamic Stability Testing*, Arnold Engineering Development Center, Vol. II, April 1965.

[2] Ericsson, L. E., "Effect of Boundary Layer Transition on Vehicle Dynamics," AIAA Paper 69-106, New York, Jan. 1969.

[3] McCauley, W. D., Saydah, A., and Beuche, J., "The Effects of Controlled Three-Dimensional Roughness on Hypersonic Laminar Boundary Layer Transition," AIAA Paper 66-26, New York, Jan. 1966.

[4] Stetson, K. F. and Rushton, G. H., "A Shock Tunnel Investigation of the Effects of Nose Bluntness, Angle of Attack and Boundary Layer Cooling on Boundary Layer Transition at a Mach Number of 5.15," AIAA Paper 66-495, Los Angeles, Calif., June 1966.

[5] Davis, F. V. and Monaghan, R. J., "Boundary Layer Measurements on 15° and 24.5° Cones at Small Angles of Incidence at $M = 3.17$ and 3.82," Rept. 2577, June 1957, Royal British Establishment.

[6] Nagamatsu, H. T. and Sheer, Jr., H. T., "Boundary Layer Transition on a 10-Degree Cone in Hypersonic Flow," *AIAA Journal*, Vol. 3, No. 11, Nov. 1965, pp. 2054–2061.

[7] Softley, E. J., "Transition of the Hypersonic Boundary Layer on a Cone," Rept. R68SD14, Oct. 1968, General Electric.

[8] Sherman, M. M. and Nakamura, T., "Flight Test Measurements of Boundary-Layer Transition on a Nonablating 22° Cone," *Journal of Spacecraft and Rockets*, Vol. 7, No. 2, Feb. 1969, pp. 137–142.